J Appl Electrochem (2014) 44:1081–1092
DOI 10.1007/s10800-014-0721-z

RESEARCH ARTICLE

A numerical assessment of bubble-induced electric resistance in aluminium electrolytic cells

Kaiyu Zhang · Yuqing Feng · Peter J. Witt · William Yang · Mark Cooksey · Zhaowen Wang · M. Phil Schwarz

Received: 7 April 2014 / Accepted: 14 July 2014 / Published online: 17 August 2014

Abstract This paper reports on an assessment of the bubble-induced electrical resistance in the Hall-Héroult process for primary aluminium production through a combined use of physical and numerical modelling. Using a physical air–water model, the transient bubble dynamics beneath the bottom surface of an anode was captured using a digital camera. Bubble morphology information obtained from the experiment was used to set up a numerical model. Computational fluid dynamics (CFD) modelling was applied to predict the current flow and the corresponding voltage drop across the electrolytic cell with and without the presence of bubbles. The predicted bubble-induced voltage drop for a current density of 0.7 A cm^{-2} is about 0.11 V for a bubble coverage of 37 % and 0.29 V for a bubble coverage of 50 %. These values are within the range of experimental measurements reported for commercial cells. The predictions show that the presence of bubbles does not greatly affect global current distribution within the whole cell, but it does significantly affect the local current flow at the anode-bath interface. Locally high current flow occurs at the contact point of the anode bottom surface, bubble and liquid. In addition to the effect of bubble coverage, the bubble size and bubble thickness affect the voltage drop significantly.

Keywords Bubble-induced electric resistance · Aluminium electrolytic cell · Numerical modelling

K. Zhang · Y. Feng (✉) · P. J. Witt · M. P. Schwarz
CSIRO Computational Informatics, Box 312, Clayton South, VIC 3169, Australia
e-mail: Yuqing.Feng@csiro.au

K. Zhang · Z. Wang
School of Metallurgical Engineering, Northeastern University, Shenyang, China

K. Zhang
School of Mechanical Engineering, Hefei University of Technology, Hefei, China

W. Yang · M. Cooksey
CSIRO Process Science and Engineering, Box 312, Clayton South, VIC 3169, Australia

1 Introduction

Despite significant advances in technology during the past century, the aluminium electrolytic cell is still the only unit for producing primary aluminium from alumina since the invention of the Hall-Héroult process in 1886. The process is highly energy intensive, requiring approximately 13 kilowatt hours (kWh) of electrical energy to produce 1 kg of aluminium, of which only about 50 % is used to decompose alumina into aluminium, the rest generating waste heat. For both cost and environmental reasons, there is pressure on the aluminium smelting industry to reduce energy consumption.

A significant contribution to the waste energy arises from CO_2 gas bubbles produced on the underside of the carbon anode acting as insulators between the anode and liquid bath. The contribution of bubbles to voltage drop is in the order of 0.25 V out of a total cell voltage of 4.0–4.6 V [1]. As shown in a recent review paper [2], the bubble-induced electrical resistance has been extensively studied in industrial cells, laboratory cells and physical models. However, despite being an intensive research topic [3–9], the detailed contribution of bubbles to voltage drop is not fully understood due to the complexity of the bubble dynamics, and the tight coupling between factors such as bubble size, bubble layer thickness and variations in cell

voltage. This incomplete understanding is reflected in the fact that published equations derived to predict bubble-induced resistance vary significantly [2]. To overcome this, we propose to investigate the detailed contribution of bubbles on electric resistance using a numerical model that can simulate the detailed current flow around the bubbles.

Numerical modelling can simulate the detailed current flow around individual bubbles and thus provide an excellent opportunity to quantitatively assess the effect of bubbles on local current distribution, and hence on induced voltage drop. Numerical techniques have been developed to study various aspects of the aluminium smelting process, such as electro-magnetic models to improve bus-bar design, thermal-electric models to improve electrical connection [10] and computational fluid dynamics (CFD) models to investigate bath flow driven by gas bubbles and/or electro-magnetic forces [11–16]. There are very limited numerical works [6, 7, 17] that investigate the electrical resistance within the presence of bubbles under the anode.

This paper presents a study in this direction. Using a two-dimensional (2D) geometry of part of a real cell as the testing bed, current flow in the domain is calculated using ANSYS/Fluent as the numerical platform. The 2D study may not fully represent the real case which is indeed three-dimensional (3D), but will give a similar trend to the 3D study, as the current mainly flows into the cell vertically and flows out through the collector bars horizontally along one direction. The 2D geometry should be acceptable as long as the 2D setting can represent the main current flows. The bubble-induced voltage drop is quantified through simulations with and without the presence of bubbles in the bath under the anode, known as the 'anode to cathode distance' (ACD). Investigations were initially conducted for different bubble coverage areas obtained from air–water physical modelling. The results of the simulations in the present work are compared with the output of various approximate models proposed in the literature. The effect of bubble size on voltage drop is further evaluated using fixed-sized bubbles uniformly distributed across the base of the anode, and the bubble thickness effect on voltage drop is studied for a fixed bubble coverage (50 %) and bubble size (16.25 mm).

2 Modelling method

2.1 Modelling methodology

To realistically model the voltage drop due to bubbles, details of the bubble profiles and coverage under the anode is required. Bubble dynamics can be obtained through an experimental setup using advanced measurement techniques or numerical modelling using surface capturing methods [12]. Recently, the bubbling dynamics in an aluminium smelting environment has been studied numerically [12–16], but fully capturing the detailed bubble dynamics is proving to be a non-trivial task with current computing facilities. In this study, an air–water physical model is used to obtain detailed bubble morphology. This bubble information is then used to set up a numerical model. Zhang et al. [12] have used numerical modelling to compare bubble behaviour in air–water and CO_2-cryolite systems. While there are some differences in detailed bubble dynamics, overall behaviour was found to be similar for both systems; such that the bubbles underneath the anode are fairly flat and the bubble layer thickness and sliding velocity in ACD are of a similar magnitude. The presence of an electro-magnetic force will affect bubble dynamics to some extent, which was not considered in that work. The bubble morphologies from the air–water model may not fully represent the CO_2 bubbles in a commercial electrolytic cell, but should be an acceptable initial approximation for studying the bubble resistance given the difficulties in obtaining the CO_2 bubble information from either plant measurements or numerical simulations.

2.2 Physical modelling

A physical air–water model was set up with the geometry representing a slice of a typical commercial Hall–Héroult prebake cell; note that the geometry is not related to any specific cell design. Figure 1 shows the main features of the model, which consists of a transparent Plexiglas container (890 × 100 × 290 mm) with a suspended box-shaped Plexiglas "anode" (650 mm in height × 100 mm in width × 240 mm in height), which fits tightly between the walls of the container. The anode box was subdivided into two equal air-tight compartments.

Air flow rate into each compartment was individually controlled to ensure a uniform gas distribution over the anode face. The distance between the anode and the bottom of the container could be adjusted. Gas evolution was simulated by passing compressed air through a micro-porous high density polyethylene plate that represented the bottom surface of the anode. The cell was fixed on a steel table with a glass tabletop and adjustable legs; this permitted the entire cell to be tilted. The tilt angle was set at 1.5° along the direction of the long edge of the anode slices (as might occur because of anode consumption), the ACD was set to 50 mm and the bath depth was 150 mm.

Changes in cell current were accounted for by varying the air flow rate through the porous polyethylene plate. In an operating cell, increased current increases reduction of alumina and increases production of CO_2 bubbles. The air injection rate of 4 L/min is equivalent to a current density of 0.39 A cm^{-2} [6, 16]. Because the physical model only represents a narrow transverse slice of a prebake cell, the

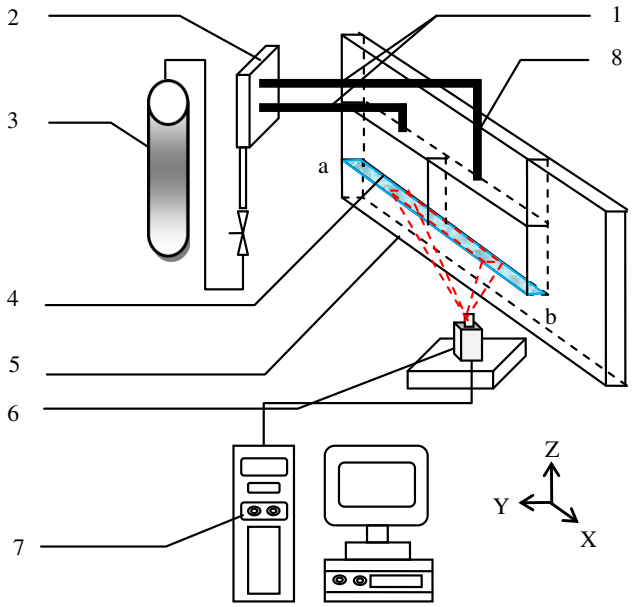

1. Pipe 2. Bubble injector regulator panel 3.Air cylinder
4. Porous panel 5. Transparent water tank 6. Camera
7. Computer 8. Anode zone
Side a: The centre of the anode Side b: The edge of the anode

Fig. 1 Schematic diagram of air–water model setup and bubble measurement arrangement

ability for bubbles to escape in the third dimension is lost. Therefore, the air bubbles beneath the anode will represent bubble behaviour of higher current density.

Measurements were performed using a high resolution digital camera that was located directly underneath the anode to capture images of the bubble morphology in the ACD. Recordings for each experimental condition were made at two locations because the camera lens field of view was insufficient to capture the whole underside of the anode.

2.3 Numerical modelling

Electrical current flow can be simulated by using different modelling methods and numerical platforms, such as finite element analysis (FEA) modelling in Abaqus and finite volume-based CFD methods in commercial codes such as ANSYS/CFX and ANSYS/Fluent. The FEA approach treats every part of the computational domain as a solid; thus, it would not be possible to simulate the dynamic motion of bubbles planned for future work. The ANSYS/Fluent software has been used in the past to study bubble dynamics [12], and has the potential to fully couple bubble flow and current flow in future work, and was therefore selected for this study.

To enable fast analysis, a two-dimensional (2D) geometry is used. Figure 2 shows the 2D geometry, which is a

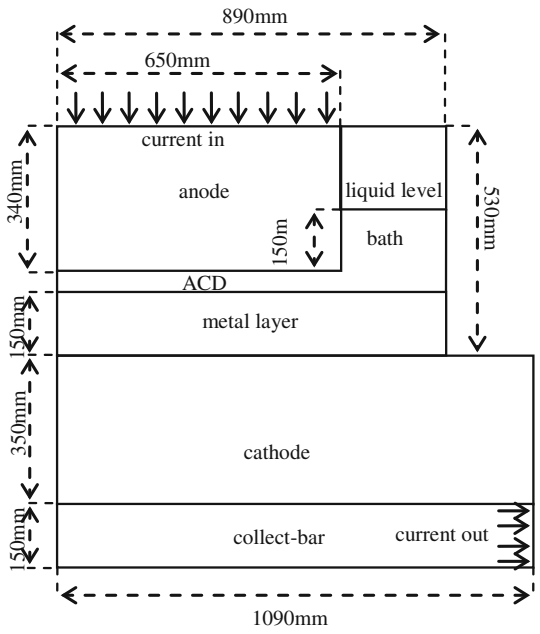

Fig. 2 Two-dimensional numerical simulation domain

cross section of the air–water model geometry. The bath domain is the same size as the physical model. To reasonably represent a real aluminium smelting process, the anode, liquid bath, metal, cathode and collector bar are included (Fig. 2). Current flows in from the top of the anode and flows out from the end of the collector bar, thus these two faces are set as an inlet and outlet for the current, respectively. The input current density is 0.7 A cm^{-2}; note that this current density is not related to any specific bubble coverage. The bubble-induced resistance is irrelevant to a specific current density; the value of 0.7 A cm^{-2} is selected to check the relevance of the predicted voltage drop to industrial cells, as most of the modern cells are operated around this current density.

To calculate additional electrical resistance induced by the presence of bubbles underneath the anode, the Laplace equation:

$$\nabla(\sigma \nabla V) = 0$$

is solved within the domain shown in Fig. 2 with bubble layer obtained from the experiments. V represents electrical potential or voltage and σ is the electrical conductivity, which varies for different materials and is provided in Table 1. The vertical boundaries at the right side and at the bottom are treated as insulating layers. The left side is set as symmetry boundary condition. At the top surface of the anode, a constant current density of 0.7 A cm^{-2} is assigned. At the right end of the collect bar where the current flows out, the value of voltage is set to zero. This setting is convenient as it allows the whole voltage drop of the full cell based on the voltage value at the anode top surface to be calculated.

Table 1 Electrical conductivity for different materials

Material	Conductivity [S m^{-1}]
Anode	2.143×10^4
Cathode	5.000×10^4
Gas	9.85×10^{-6}
Cryolite	2.220×10^2
Steel	7.587×10^5
Metal	4.167×10^5

The commercial CFD package ANSYS/Fluent, which is based on the Finite Volume Method, was used as the numerical modelling tool. As noted earlier, the longer term plan is to resolve the bath and bubble motion while simultaneously predicting the electrical current distribution. Thus, the transient volume of fluid (VOF) model with an additional user-defined scalar equation for the electrical potential is used in this work. Using such a setup in Fluent requires the Navier–Stokes equation to be solved for the bath and gas flow as well as the volume fraction. As the present work focuses on predicting the electrical current flow for specific bubble distributions captured in physical modelling, only the scalar equation (V) needs to be solved. Thus, the flow calculation is only performed for one small time step (10^{-50} s), given that the velocity is of the order 0.1 m s^{-1}, the bubble and flow field do not change significantly during this time step, and the approach is equivalent to freezing the motion of the bubbles. The solved scalar equation is equivalent to solving the Laplace equation for the electrical potential at an instant in time for an instantaneous bubble configuration. Further work with continuous injection of gas, extension to three dimensions and solution of larger multiple time steps is needed to better represent the aluminium smelting process and to quantify the fluctuations in voltage drop and current distribution variation with time and changing flows. However, such a modelling exercise would require greatly increased computational resources.

In setting up the model, the following simplifications are made:

- The bubble information in the side channels is not included due to the difficulty of measurement. It is believed that bubbles in the side channel have only a small effect on voltage drop as the current mainly flows through the ACD;
- The effects of temperature and alumina concentration on the electrical conductivity is not considered: fixed values given in Table 1 are set for each of the cell materials, the cryolite and the liquid metal;
- The model is run for a number of different time instants to give information on different bubble states. The effect of liquid motion on current flow is neglected, with the assumption that voltage and gas distribution are the dominant factors in determining current flow.

The mesh is built using ANSYS/Mesh and refined at the interface of the bubble and around the underside of the surface, allowing detailed current flow paths around the bubbles to be more accurately captured. Settings used in meshing the model are maximum cell surface area which is set as 5×10^{-6} m^2 and the minimal cell surface area which is set as 6.0×10^{-9} m^2. Thus, the boundaries for the minimum bubble size (1 mm) and the maximum bubble size (5 mm) can be clearly defined. The absolute convergence criteria for continuity, scalar and velocity equations are set as 10^{-7} to ensure simulation accuracy.

As listed in Table 2, a total of 15 cases were simulated. Cases A, B and C correspond to the bubble sizes and locations captured from the air–water model at three instants when the gas flow rate was 4 L min^{-1}, and cases D, E and F for three instants when the gas flow rate was 8 L min^{-1}. Case G represents the condition without bubbles, which is used as the baseline to quantify the bubble-induced voltage drop. Cases H, I and J represent three artificial conditions, each with 50 % bubble coverage and a uniform bubble size. These three cases are used to assess the effect of bubble size on voltage drop. Case K is to investigate an unusual cell operating condition, known as an anode effect, with 100 % bubble coverage. Based on the same uniform bubble size as case J, cases L, M, N and O are to evaluate the effect of bubble thickness on voltage drop.

3 Results and discussion

3.1 Bubble measurement in ACD

Figure 3 plots the bubble shape on the underside of the anode at three time instants for a gas flow rate of 4 L min^{-1} (Fig. 3a, b, c) and 8 L min^{-1} (Fig. 3d, e, f). Due to the different reflections of gas and liquid, bubble boundaries can be clearly distinguished, i.e. the bubble region is brighter than the bubble free region.

Following the injection of air through the porous anode base, small tiny bubbles start to appear randomly on the underside of the anode. These tiny bubbles start to grow with the continuous injection of gas. When a bubble is sufficiently large, it starts to slide towards the high end of the anode due to the buoyancy effect. During the sliding process, the bubble contacts bubbles within its path and they coalesce to form a larger bubble. This coalescence process results in much larger bubbles at the higher end of the anode (side b) than at the low end of the anode (side a). This phenomenon was described as a "sweeping effect"

Table 2 Bubble information obtained from the air–water physical model and used to set up the 2D model

Simulation cases	Gas flow rate (L min^{-1})	Anode bubble coverage (%)	Number of bubbles	Bubble size (mm)	Bubble thickness (mm)	Purpose
A	4	37	20	Varied	5	Effect of bubble coverage
B	4	40	22	Varied	5	Effect of bubble coverage
C	4	36	18	Varied	5	Effect of bubble coverage
D	8	50	19	Varied	5	Effect of bubble coverage
E	8	47	13	Varied	5	Effect of bubble coverage
F	8	46	17	Varied	5	Effect of bubble coverage
G	–	0	0	–	–	Base case
H	–	50	5	65	5	Effect of bubble size
I	–	50	10	32.5	5	Effect of bubble size
J	–	50	20	16.25	5	Effect of bubble size
K	–	100	1	650	5	Effect of very large bubbles
L	–	50	20	16.25	3	Effect of bubble thickness
M	–	50	20	16.25	4	Effect of bubble thickness
N	–	50	20	16.25	6	Effect of bubble thickness
O	–	50	20	16.25	7	Effect of bubble thickness

[18]: in this way, the bubbles grow in size and gain speed during a typical coalescing process.

The grey scale photographic images were converted to black-and-white images using the light intensity filter function in the Photoshop software and are shown under the photographs in Fig. 3. From these images, the bubble boundaries can be identified clearly. In the present two-dimensional slice model, bubble information at the centreline of the slice, i.e. the anode width direction (red line in Fig. 3), was used to determine the bubble size in the model. This was achieved by setting the gas volume fraction in the model corresponding to the bubble fraction along the red line in Fig. 3.

As the photographs only capture two-dimensional images of the bubbles, the bubble thickness cannot be obtained directly. From the experiment, it is not straightforward to determine the bubble layer thickness or three-dimensional shape. Some simplification of the shape is made in the numerical model setup. The body of the bubble is assumed to be parallel with the anode base and the head and tail are assumed to be of a constant radius. Using a probe that transfers a signal when it occasionally contacts a gas bubble, Haupin [1] found the gas bubble layer thickness under the anode in a real cell to be approximately 5 mm. From visual observations, the bubble layer thickness in the air–water model was observed to be of a similar value [20]. Accordingly, the bubble layer thickness in the model was set to 5 mm with the length varied to account for different bubble sizes. It is reported that the contact angle of molten electrolyte on a graphite sample was measured to be around 120° [19, 20]. Hence, the geometry of the bubble head and tail is constructed to fit this angle. For bubbles with a diameter less than 5 mm, the parallel region of the bubble was not constructed and bubble consisted of only the head and the tail. Following these simplifications, the 2D bubble profile is sketched below each black-and-white image in Fig. 3.

Table 2 A–F lists some of the statistical bubble information obtained from the experiments. Bubble coverage is about 40 % at the lower gas flow rate of 4 L/min (Table 2A–C) and about 50 % when the gas flow rate is doubled (Table 2D–F). These values agree reasonably well with the past experimental work [21]. Measured results show that the bubble coverage varies with time, but remains within a range around ± 10 % for each flow rate.

3.2 Numerical modelling

Table 3 lists the bubble-induced resistance for all simulation cases. For comparison with conventional industrial cell operating conditions, the resultant bubble-induced voltage drop and the total voltage drop is provided for a current density of 0.7 A cm^{-2} [22].

3.2.1 Effect of bubble coverage

In the simulations presented here, the same total current was used for both gas generation rates. This might underestimate the contribution of gas coverage to voltage drop, as a high gas coverage often results in a high current density at the anode bottom surface [2]. Therefore, instead of comparing the value of voltage drop, it is more reasonable to compare the bubble-induced resistance, which is commonly used in the literature.

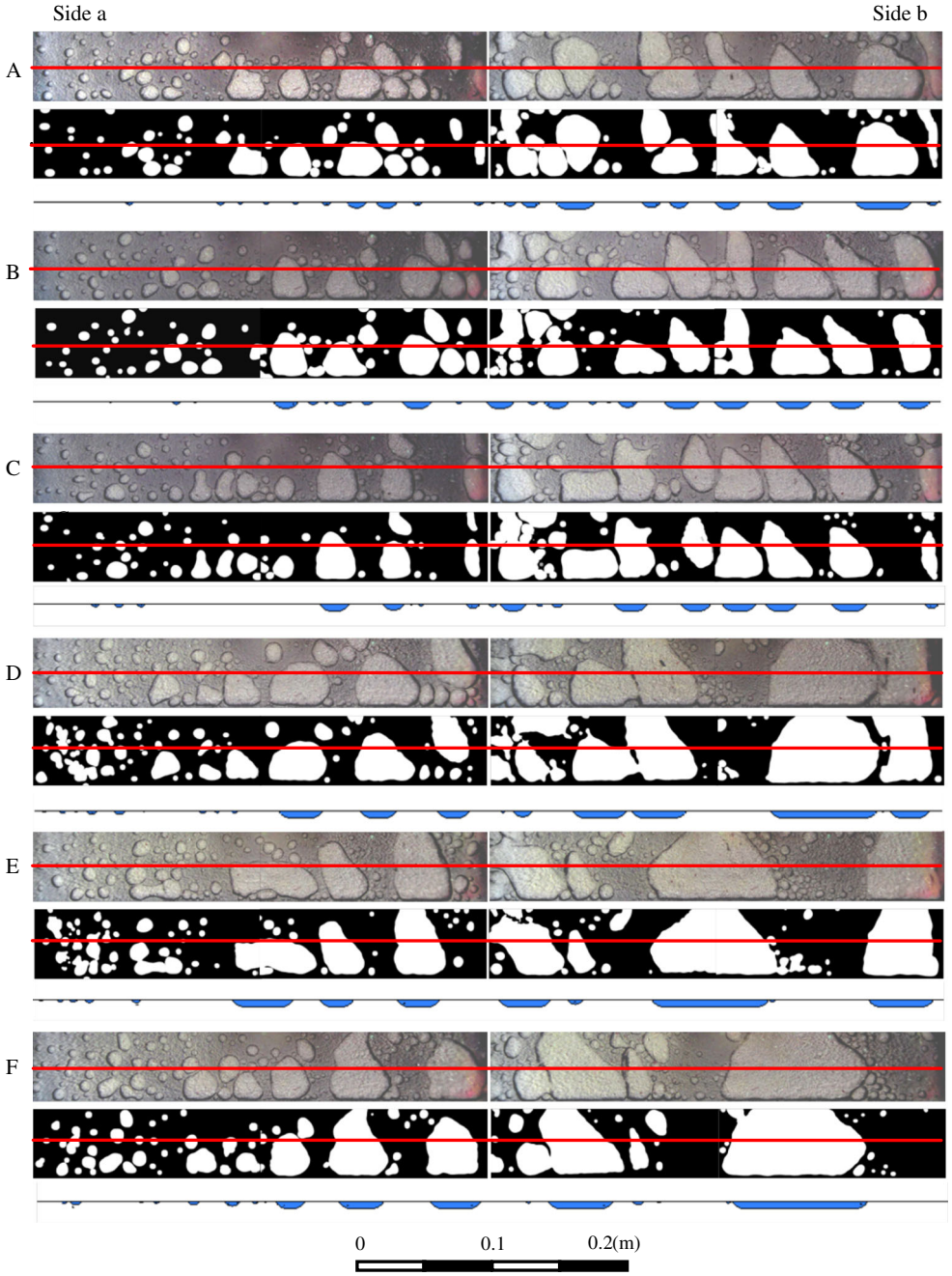

Fig. 3 Snapshots of bubble morphology in ACD: **a**, **b**, **c** represent three instants when the gas flow rate is 4 L/min, and **d**, **e**, **f** represent three instants when the gas flow rate is 8 L/min. The bubble information at the red line is used for 2D numerical model setup

Resistance of electrolyte in the ACD without bubbles can be obtained from the resistivity of electrolyte (k_0), anode–cathode distance (H) and the area of the anode bottom (A) as $\frac{k_0}{A} \times H$. When a bubble is present, the resistance in ACD can be expressed as the sum of the resistance of gas/electrolyte layer and the resistance of pure electrolyte in lower part of ACD. Table 4 summarises existing bubble resistance equations derived from both experimental work and theoretical investigation. Equation (1) uses a linear relationship between bubble layer conductivity and bubble coverage [2], while Eqs. (2, 3 and 4) treat the relationship non-linear with different expressions [23] [24]. In Eq. (5), an effective resistivity (k_{eff}) for the whole electrolyte in ACD zone is defined [25].

Figure 4 compares the simulated bubble resistance with these different equations. The predicted bubble resistances are similar to those predicted by these equations, but the trend does not fit to any particular equation. At the lower bubble coverage, the predicted value agrees well with Eqs. 2 and 5; while Eqs. 1 and 3 underestimate the bubble-

Table 3 Bubble-induced resistance and voltage drop at a constant current density of 0.7 A/cm^2

Simulation cases	Bubble-induced resistance [ohm]	Bubble-induced voltage drop [v]	Total voltage drop [v]
A	0.000248	0.143	1.532
B	0.000286	0.160	1.549
C	0.000233	0.137	1.526
D	0.000590	0.313	1.702
E	0.000640	0.323	1.712
F	0.000578	0.298	1.687
G	0	0	1.393
H	0.001123	0.511	1.9
I	0.000648	0.311	1.7
J	0.000426	0.178	1.567
K	0.024719	11.247	12.636
L	0.000363	0.157	1.546
M	0.000391	0.170	1.559
N	0.000437	0.192	1.581
O	0.000470	0.203	1.592

induced resistance, and the Eq. 4 overestimates the bubble resistance. At the higher bubble coverage, all the equations underestimate the bubble resistance. The predicted increase rate of the resistance as a function of the bubble coverage is higher than these equations. The predicted values offer a good opportunity to propose a new equation for a better prediction of the bubble-induced resistance. Considering the proposed equation should be for general use, more simulations to consider bubble coverage below 45 % and above 55 % are required. Also, though it is believed that the 2D case can reasonably represent the 3D situation, it is better to quantify any difference between 2D and 3D simulations before proposing a new equation. Thus, a more detailed model with 3D simulations should be performed before forming a new equation.

In addition to quantifying the bubble-induced resistance, it is interesting to examine how the bubbles affect the voltage drop and current flow. Figure 5(a) shows the predicted voltage profile without the presence of a bubble layer (i.e. case G in Table 2), and Fig. 5(b) shows results for a bubble layer as in case A in Table 2. Clearly, the presence of a bubble layer leads to a higher voltage drop across the cell. The total voltage drop is about 1.39 V without the presence of bubbles and 1.53 V with the presence of bubbles. As shown by the contour map, the highest voltage gradient occurs in the bath region, indicating that most energy loss due to electrical resistance occurs in the bath. The voltage drop over the bath layer and different lining materials are listed in Table 5 for case G. The predicted voltage drop across different components of the cell is consistent with the literature [26], demonstrating that the simplified 2D model used in this work gives a reasonable prediction of real cell conditions.

The influence of bubbles is further investigated by plotting the current flow distribution. Figure 6(a) plots the current flow in the full simulation domain without the

Table 4 Published equations for the calculation of bubble-induced electrical resistance

NO	Resistivity of different part	Resistance with bubble	the extra resistance due the existing bubble	Ref.
1	$k_G = k_0 \times \frac{1}{(1-f)}$	$\frac{k_G}{A} \times d_b + \frac{k_0}{A} \times (H - d_b)$	$\Delta R = k_0 \times d_b \times (1/(1-f) - 1)/A$	[2]
2	$k_G = k_0 \times (\frac{1+f/2}{1-f})$	$\frac{k_G}{A} \times d_b + \frac{k_0}{A} \times (H - d_b)$	$\Delta R = k_0 \times d_b \times ((1+f/2)/(1-f) - 1)/A$	[22]
3	$k_G = k_0 \times (1 + (0.9015) \times \frac{3}{2} \times f)$	$\frac{k_G}{A} \times d_b + \frac{k_0}{A} \times (H - d_b)$	$\Delta R = k_0 \times d_b \times 1.3524 \times f/A$	[22]
4	$k_G = k_0 \times (1-f)^{-1.5}$	$\frac{k_G}{A} \times d_b + \frac{k_0}{A} \times (H - d_b)$	$\Delta R = k_0 \times d_b \times ((1-f)^{-1.5} - 1))/A$	[23]
5	$k_{eff} = \frac{k_0}{H} \times ((H - d_b) + d_b \times (1 - 1.26f)^{-1})$	$\frac{k_{eff}}{A} \times H$	$\Delta R = k_0 \times d_b \times (1/(1 - 1.26 \times f) - 1)/A$	[24]

ΔR: the extra resistance due the presence of bubbles
k_0: the resistivity of the cryolite
k_G: the resistivity of the gas-cryolite layer
k_{eff}: the effective resistivity of cryolite in ACD zone
d_b: the depth of the bubble layer
f: the fractional surface coverage by bubbles
A: the area of the underside surface of anode
H: the depth of ACD
$\frac{k_0}{A} \times H$: the resistance without bubble

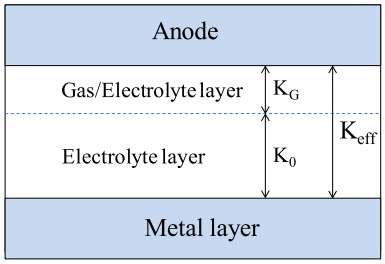

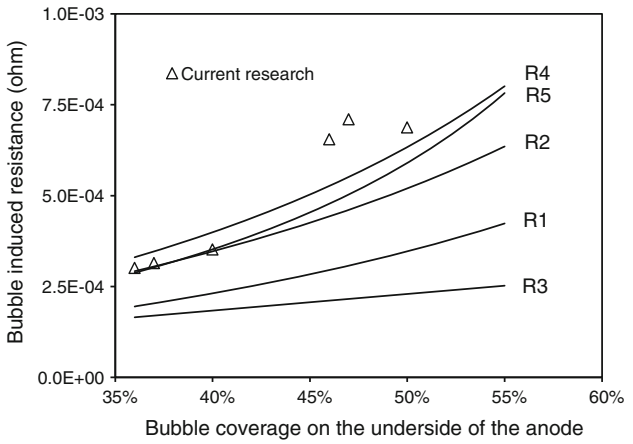

Fig. 4 Comparison between predicted bubble resistance and published equations

presence of a gas bubble layer. The current flow is almost uniformly downward in the anode and ACD, with only a small current in the side channel. In the metal layer, a strong horizontal component to the current flows is predicted. This is due to the high conductivity of the metal layer and low voltage potential on the side of the collector bar. As the current passes through the cathode, it changes to a horizontal direction and flows out through the end of the collector bar. The predicted current flow when a bubble layer is present under the anode is shown in Fig. 7. Comparing the results in Fig. 7a to those in Fig. 6a shows that the overall current flow is similar in both cases. This implies that the presence of a bubble layer does not make a significant change to the overall current flow in the cell.

Figures 6b and 7b show a close-up view of current flow at the anode-bath interface without and with the presence of a bubble layer, respectively. Without the bubble layer (Fig. 6b), the current distribution is quite uniform. When a bubble layer is present, increased resistance from the gas layer prevents current from directly passing through the bubble. Current in the anode above the bubble changes direction and flows through gaps between the bubbles. Consequently, a high local concentration of current density occurs at the contacting point at the intersection of the anode, gas and bath. It is easy to understand that bubbles reduce the area for current flow, thereby increasing the resistance and local current density, leading to an extra voltage drop which is regarded as the bubble-induced voltage drop.

3.2.2 *Effect of bubble size*

Both the predicted voltage drop data and the bubble resistance data (Table 3; Fig. 4) show that higher bubble coverage generally corresponds to a higher bubble resistance. Case D shows an exception to this trend: the coverage is higher than case E, but the predicted voltage drop is lower than case E. Table 2 shows that the number of bubbles in case D is higher than in case E and thus the

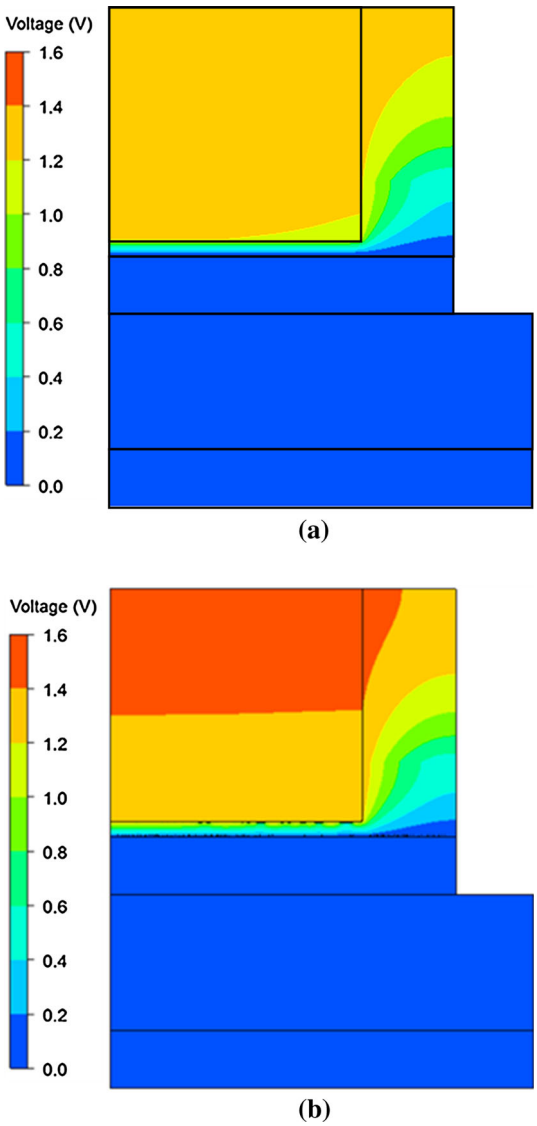

Fig. 5 Voltage distribution: **a** without the presence of bubbles, **b** with the presence of bubbles for the case shown in Fig. 3a

Table 5 Voltage drop across each component of an aluminium reduction cell without the presence of a bubble layer

Region	Voltage drop (v)
Anode	0.2239
Bath	1.1004
Metal	0.0015
Cathode	0.0464
Collect bar	0.0203
Total	1.3926

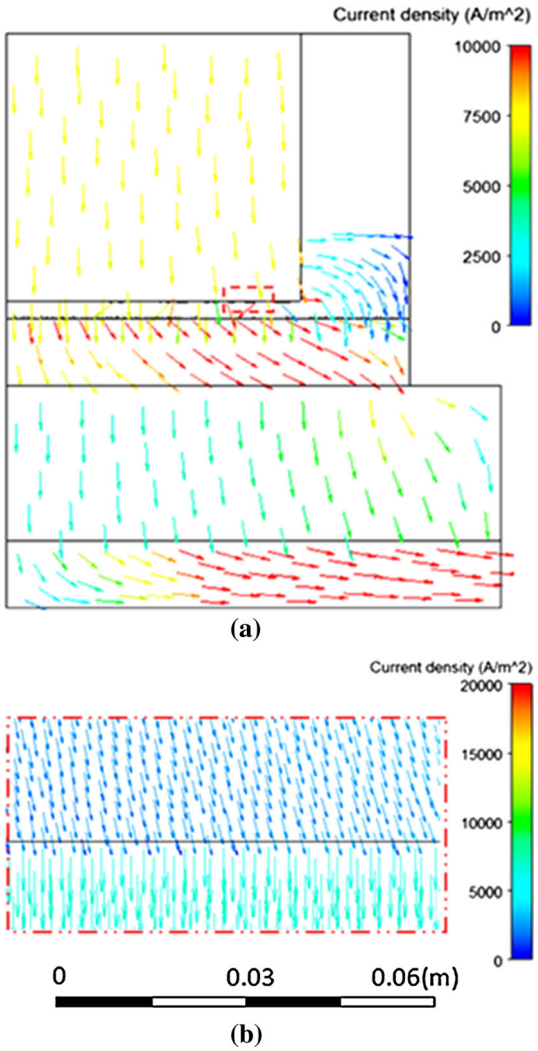

Fig. 6 Current flow without the bubble layer for Case G: **a** full simulation domain, **b** a close-up view near the anode-bath interface

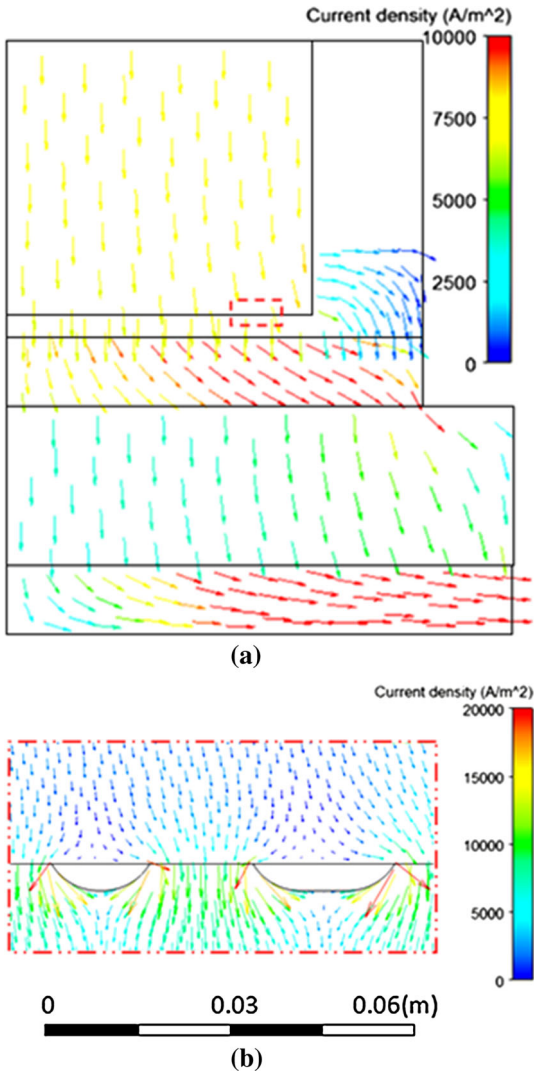

Fig. 7 Current flow with the presence of the bubble layer for Case A: **a** full simulation domain, **b** a close-up view near the anode-bath interface

bubble size is smaller. This suggests that the bubble size may contribute to differences in resistance. To confirm this, three more simulations (case H, I and J in Table 2) are conducted with the same bubble coverage, but different bubble sizes (65, 32.5 and 16.25 mm, respectively). As the bubble coverage is set to 50 %, the gap between bubbles is the same as the bubble size. This artificial treatment of bubble size and its distribution cannot be fully representative of a real case, but as a proof-of-concept study, this treatment will be effective in highlighting the bubble size effect.

Figure 8 plots the predicted voltage profile over the full simulation domain for the cases H, I and J. It is clear that the bubble-induced resistance is significantly influenced by the bubble size. The larger size bubbles lead to a higher bubble resistance, increasing from 0.000426 ohm at bubble size 16.25 mm to 0.001123 ohm at bubble size 65 mm. The results indicate that the additional bubble-induced voltage drop is not only affected by bubble coverage, but is also strongly affected by bubble size. A possible reason is that when the bubble size is larger, the current needs to travel a longer distance to bypass the bubble region, leading to higher voltage drop. This can be confirmed by plotting the current flow. For the three cases investigating the bubble size effect (case H, I, J), the global current flow patterns are very similar to the flow patterns shown in Figs. 6a and 7a. Thus, only the current flow near the anode-bath interface is plotted here. Figure 9 shows a close-up view of the current flow near the anode-bath interface. Consistent with the findings in Fig. 7b, a high local concentration of current density occurs at the contacting point at the intersection of the anode, gas and bath. The local concentration reduces as the bubble size reduces.

These results demonstrate that it is necessary to consider the bubble size effect in quantitative prediction of the

bubble resistance. In the literature, there are many equations that correlate bubble coverage with current density. As stated in a recent paper [27], the simple equations are not sufficiently comprehensive, as bubble coverage is controlled by a multitude of factors, such as anode surface properties, size of the anode, wettability between anode surface and bath and the bubble surface tension. In a real cell, the surface tension is strongly affected by local concentrations of alumina. Thus, quantifying relationships for bubble coverage and bubble size in an actual cell is even more difficult. A study on bubble coverage and bubble size would be of practical importance, a topic challenging the aluminium research community.

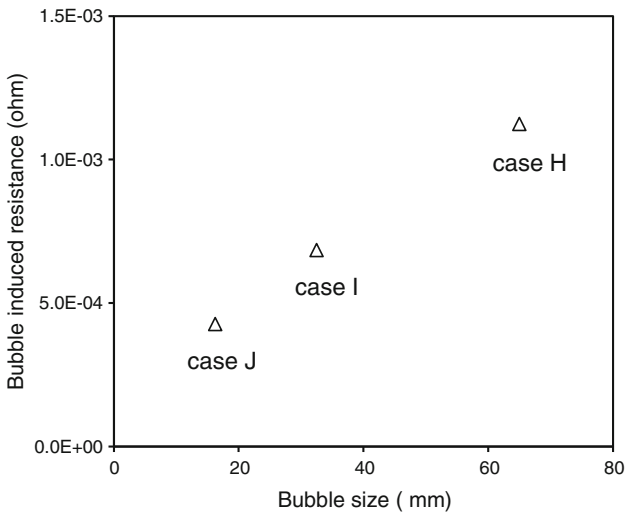

Fig. 8 Bubble resistance for different bubble sizes when the bubble coverage is fixed at 50 %

Detailed bubble behaviour is believed to be very complex in real cell operation as bubble coalescence is a significant factor. Occasionally, very large bubbles may form, such as during an anode effect, and it is of interest to quantify the effect on cell current flow and voltage when a very large bubble is in the ACD. A case with 100 % bubble coverage in the ACD (case K in Table 2) is simulated to examine this question. Figure 10 plots the global current flow for this case: the high resistance of the bubble layer causes the current to flow through the side of the anode and into the side channel of the bath. Once the current bypasses the bubble layer, some of the current flows back towards the centre region in the metal layer. For this case, the current flow is markedly different to the other cases where the current mainly flows downward in the bath towards the metal layer (Figs. 6a, 7a). Consequently, bubble resistance is almost 50 times higher than the other cases. Current flow in the cathode and collector region shows a similar pattern to the other cases (Figs. 6a, 7a).

3.2.3 *Effect of bubble thickness*

To understand the effect of bubble thicknesses on bubble resistance, four extra cases (L, M, N and O) are simulated with bubble thickness 3, 4, 6 and 7 mm, respectively, for bubble coverage 50 % and bubble size 16.25 mm. The bubble resistances calculated from these cases, together

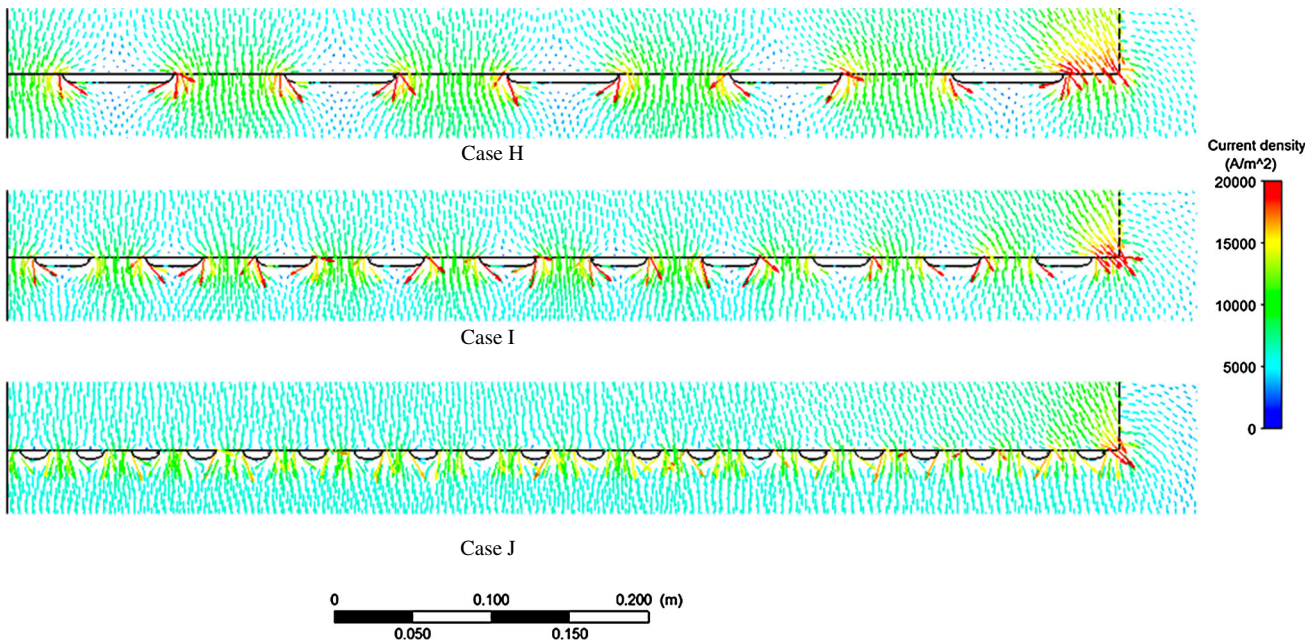

Fig. 9 A close-up view of the current flow near the anode-bath interface for the cases H, I and J in Table 2

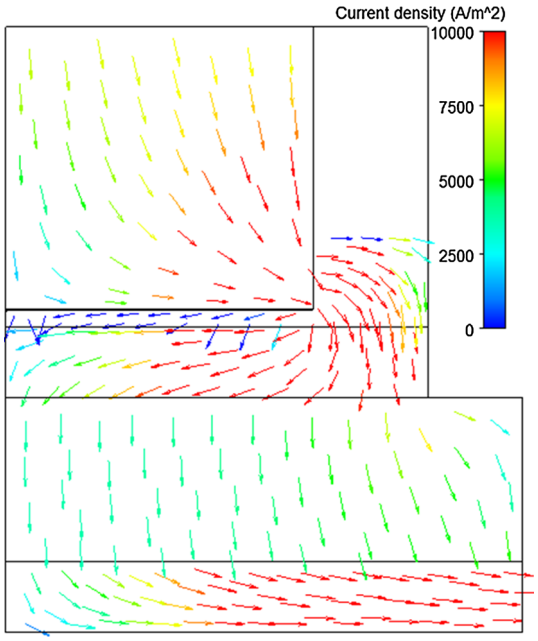

Fig. 10 Current flow pattern with the presence of bubble layer which covers the whole anode underside

with case J, are plotted in Fig. 11. As expected, the bubble resistance increases as the bubble thickness increases. It is interesting to see that the relationship between bubble resistance and bubble thickness is almost linear. It is expected that for typical values of the ACD (viz. 50 mm), variation of a few millimetres in bubble thickness will not affect the current flow distribution significantly. It is likely that bubble thickness will have a stronger effect on bubble resistance as the ACD reduces.

The detailed current flow predictions show that current is not uniform near the bubbles. This indicates that the Lorentz force, which is a function of current density, will also be non-uniform near the bubble interfaces, and this may substantially affect bubble motion. In the present model, neither bubble dynamics nor the Lorentz force is included. In future work, it is worthwhile to investigate the effect of these variations in current density on bubble motion.

4 Conclusions

Bubble-induced electrical resistance and the detailed current flow in the Hall-Héroult process have been numerically investigated using a two-dimensional geometry representative of part of an aluminium cell. The main findings from this study are as follows:

- The predicted voltage drop due to bubbles is approximately 0.15 V for a bubble coverage of 37 % and 0.3 V for a bubble coverage of 50 % when the current density is set to 0.7 A cm^{-2}. These values are in reasonable agreement with the experimental measurements.
- The predicted bubble-induced resistances are within the range of published equations, but do not fit any of the published expressions. The predicted increase rate of the resistance as a function of the bubble coverage is higher than these equations.
- The presence of bubbles (bubble coverage <50 %) does not greatly affect the global current flow in the whole cell, but it does significantly affect the local current distribution at the anode-bath interface. Local high current flow occurs around the contact point of the anode bottom surface, bubble and liquid.
- The bubble size (for a fixed bubble coverage) significantly influences the bubble-induced voltage drop and local current distribution. Both the bubble-induced resistance and local current concentration increase as the bubble size increases.
- If the whole anode underside is covered with a large bubble, as in an anode effect, most current would flow out from the side surface of the anode and create a high current density in the side channel, which causes substantial energy loss. Quantitatively, under such situation, the gas-induced voltage drop can exceed 10 V.
- For a fixed bubble coverage, the bubble-induced resistance increases as the bubble thickness increases.

Simulation results obtained demonstrate the feasibility of the present modelling approach as an effective numerical tool for the study and prediction of bubble-induced electrical resistance. Further numerical modelling studies including of bubble motion in the presence of Lorentz force will be conducted to fully assess the bubble-induced resistance in detail.

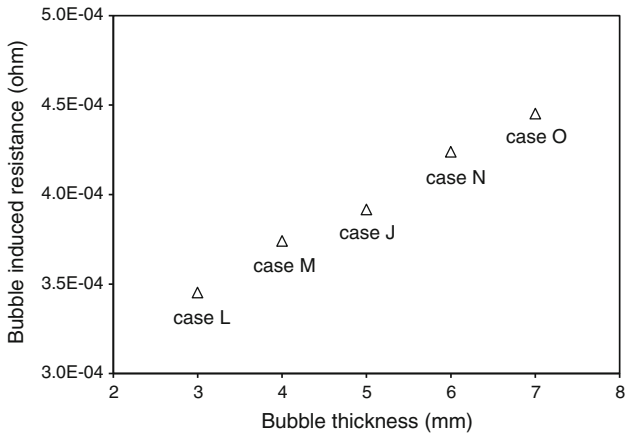

Fig. 11 Bubble resistance for different bubble thicknesses when the bubble coverage is 50 % and the bubble size is 16.25 mm

Acknowledgments The work is financially supported by CSIRO Minerals Down Under Flagship. Kaiyu Zhang thanks the China Scholarship Council (CSC) for a visiting PhD scholarship and the China Nature Science Foundation Grant under Grant No: 51228401.

References

1. Haupin W (1971) Scanning reference electrode for voltage contours in alumium smelting cells. J Met 23:46
2. Cooksey MA, Taylor MP, Chen JJJ (2008) JOM 60:51
3. Kasherman D, Skyllas-Kazacos M (1988) J Appl Electrochem 18:863–868
4. Qian K, Chen JJJ, Matheou N (1997) J Appl Electrochem 27:434–440
5. Qian K, Chen ZD, Chen JJJ (1998) J Appl Electrochem 28:1141–1145
6. Zoric J, Solheim A (2000) J Appl Electrochem 30:787–794
7. Perron AL, Kiss LI, Poncsak S (2006) J Appl Electrochem 36:1381–1389
8. Perron AL, Kiss LI, Poncsak S (2007) J Appl Electrochem 37:303–310
9. Alam M, Yang W, Mohanarangam K, Brooks G, Morsi YS (2013) Metall Mater Trans B 44B:1155–1165
10. Molenaar D, Ding K, Kapoor A (2011) Light metals 2011. TMS, Warrendale 985
11. Feng YQ, Cooksey M, Schwarz MP (2011) Light metals 2011. TMS, Warrendale 543
12. Zhang KY, Feng YQ, Schwarz MP, Wang ZW, Cooksey MA (2013) Ind Eng Chem Res 52:11378–11390
13. Wang Q, Li BK, He Z, Feng NX (2013) Metall Mater Trans B
14. Das A, Morsi Y, Brooks G, Yang W, Chen JJJ (2011) 10th Australasian aluminium smelting technology conference, Launceston, Tasmania, Australia, October 09–14
15. Wang YF, Zhang LF (2010) Light metals 2010. TMS, Seattle 14
16. Einarsrud KE (2010) Metall Mater Trans B-Process Metall Mater Process Sci 41:560
17. Einarsrud KE, Johansen ST (2011) 8th International conference on CFD in the oil, gas, metallurgical and process industries, Trondheim, Norway, 21 June 2011
18. Fortin S, Gerhardt M, Gesing AJ (1984) J Met 35:92
19. Grjotheim K, Krohn C, Thonstad J (1982) Aluminium electrolysis: fundamentals of the Hall-Héroult process, Dusseldorf, Germany, p. 146
20. Cassayre L, Utigard TA, Bouvet S (2002) J Met 41–45
21. Aaberg RJ, Ranum V, Williamson K (1997) Light Met 341
22. Zhuxian Qiu (2006) Nonferrous Metal Metallurgy, P51. Metallurgical Industry Press, Beijing
23. Sides PJ, Tobias CW (1982) J Electrochem Soc 129(12):2715–2720
24. Solheim A, Thonstad J (1986) Light Met 397
25. Houston GJ, Taylor MP,Williams DJ, Grjotheim K (1988) Light Met 641–645
26. Grjotheim K, Welch BJ (1980) Aluminium Smelter Technology: A pure and applied approach. Aluminium-Verlag GmbH, Dusseldorf
27. Vogt H (2012) Electrochim Acta 78:183